ADVANCED HEALTHCARE MATERIALS
www.advhealthmat.de

In Vivo Accumulation of Regulatory T Cells Using Eliglustat-Loaded Cryogels

Einat. B. Vitner, Giovanni Bovone, Wei-Hung Jung, Junzhe Lou, Hugh Hankenson, Mason T. Dacus, Yoav Binenbaum, Kwasi Adu-Berchie, Alexander G. Stafford, Miguel C. Sobral, and David J. Mooney**

Regulatory T cells (T_{regs}) maintain immune homeostasis and their adoptive transfer is being widely explored to mitigate inflammatory and autoimmune conditions. Here a biomaterial is developed to accumulate T_{regs} at a specific anatomic location to bypass the need for ex vivo T_{reg} isolation and adoptive transfer. It is first shown that eliglustat, an FDA-approved inhibitor of UDP-glucose ceramide glucosyltransferase, promotes T_{regs} from both naïve and activated $CD4^+$ T cells in vitro. Click-crosslinked cryogels fabricated from alginate and collagen allow for a sustained release of CXCL10 or CXCL11, and when injected in subcutaneous tissues led to the enrichment of effector and memory T cells to the scaffolds. Loading eliglustat into these cryogels significantly enhances the local accumulation of T_{regs} in vivo. These findings demonstrate that eliglustat-loaded cryogels offer a simple yet effective biomaterial strategy to boost T_{reg} directly in vivo, potentially providing a targeted method to treat various inflammatory and autoimmune diseases.

1. Introduction

Immune system imbalances contribute to a wide range of diseases, including cardiovascular disorders, diabetes, Alzheimer's disease, asthma, and autoimmune conditions.[1] CD4+ regulatory T cells (T_{regs}) play a crucial role in maintaining immune homeostasis and preventing autoimmune responses by suppressing excessive immune activation. While adoptive transfer with polyclonal T_{regs} has shown promise, recent studies suggest that T_{regs} are particularly effective in regulating and improving immune tolerance in a disease-specific manner.[2] However, the isolation, culture, and expansion of T_{regs} present significant challenges: these processes are costly, require specialized techniques and facilities. An attractive alternative is the direct in vivo accumulation of immunosuppressive T_{regs}.[3] In spite of significant efforts, an effective method to accumulate T_{regs} in vivo remains a significant unmet challenge in the field.[4]

While $Foxp3^+$ T_{regs} can be generated from naïve T cells through antigen stimulation in the presence of transforming growth factor-β (TGF-β) and interleukin (IL)-2, these factors are insufficient to generate T_{regs} from T effector (T_{eff}) and T effector memory (T_{em}) cells.[5] Currently, cyclin-dependent kinase 8/19 (CDK8/19) inhibitors are the only known class of drugs capable of generating T_{regs} from $T_{eff/em}$ cells.[6] Biomaterials have also been explored for their potential in T_{reg} cell accumulation. Poly(lactide-co-glycolide) (PLG) particles have been used to accumulate T_{regs} in vivo by presenting antigens at low dosages.[7] Scaffolds can also be utilized as local niches for immunomodulation where T cells or antigen-specific cells are concentrated.[8] These approaches have also been investigated to deliver immune cells. For instance, PLG scaffolds were used to deliver T_{regs} and pore-forming hydrogels employed to recruit and stimulate dendritic cells, indirectly promoting T_{regs} formation.[9–12]

We explore the potential of modulating sphingolipid metabolism to induce T_{regs}. Sphingolipids, essential components of eukaryotic cell membranes, have recently gained attention for their role in regulating chronic inflammation and T cell activation and function.[13–19] UDP-glucose ceramide glucosyltransferase (UGCG), the initial enzyme in glycosphingolipid biosynthesis, plays a pivotal role in regulating sphingolipid metabolism. Among these, eliglustat (EGT) is a an UGCG inhibitor drug approved by the Federal Drug Administration (FDA) for treating Gaucher disease and its effect on T cell is currently unexplored.[20]

E. B. Vitner, G. Bovone, W.-H. Jung, J. Lou, H. Hankenson, M. T. Dacus, Y. Binenbaum, K. Adu-Berchie, A. G. Stafford, M. C. Sobral, D. J. Mooney
John A. Paulson School of Engineering and Applied Sciences
Harvard University
Cambridge, MA 02138, USA
E-mail: evitner@seas.harvard.edu; mooneyd@seas.harvard.edu

E. B. Vitner, W.-H. Jung, J. Lou, M. T. Dacus, Y. Binenbaum, K. Adu-Berchie, A. G. Stafford, D. J. Mooney
The Wyss Institute for Biologically Inspired Engineering Harvard University
Boston, MA 02138, USA

E. B. Vitner
Department of Biochemistry and Molecular Genetics
Israel Institute for Biological Research
Ness-Ziona, Israel, 7410001

Y. Binenbaum
Dana-Farber/Boston Children's Cancer and Blood Disorders Center
Boston MA 02115, USA

The ORCID identification number(s) for the author(s) of this article can be found under https://doi.org/10.1002/adhm.202501529

DOI: 10.1002/adhm.202501529

Here, we demonstrate that EGT not only induced naïve $CD4^+$ T cells to differentiate into T_{regs} but it also promoted the regulatory phenotype in activated $CD4^+$ T cells. In vitro, the formed T_{regs} were functional in suppressing T cell proliferation. To enhance the immunosuppressive effect of EGT in vivo, we developed a porous biomaterial to locally enrich $T_{eff/em}$ cells by releasing chemoattractants. When subcutaneously injected in mice, EGT released from the scaffolds successfully promoted T_{reg} accumulation. This strategy offers a straightforward yet effective means to generate T_{regs} in vivo, potentially opening new avenues for immunomodulatory therapies.

2. Results and Discussion

2.1. Eliglustat is a Foxp3 Inducer in Naïve T Cells

We first evaluated the effect of EGT on the viability and proliferation of $CD4^+$ T cells (Figure S1a, Supporting Information). EGT led to a decrease in cell viability at concentrations higher than 40 uM. EGT exposure at lower concentrations induced Foxp3 expression in naïve murine $CD4^+$ and $CD8^+$ T cells. Murine naïve T cells were stimulated with anti-CD3/anti-CD28 beads, IL-2, in the presence or absence of TGF-β (0.5 ng mL^{-1}) or EGT (10 μM). EGT-treatment during activation significantly increased Foxp3 mean fluorescence intensity (MFI) and $Foxp3^+$ cell frequency in both $CD4^+$ and $CD8^+$ populations (**Figure 1**a,b). A combination of EGT and TGF-β synergistically increased Foxp3 MFI and $Foxp3^+$ cell frequency in $CD4^+$ T cells. The higher percentage of T_{regs} ($Foxp3^+$) among the $CD4^+$ and $CD8^+$ T cells in response to EGT was due to an increase in T_{reg} cell number and a decrease in the number of $Foxp3^-$ cells (Figure 1c; Figure S2, Supporting Information). The ratio of T_{reg} $CD4^+$ T cells, compared to other helper T cell subsets, coordinately increased (Figure S3, Supporting Information). EGT was not toxic to $Foxp3^-$ cells at the concentration used to induce Foxp3 activity (Figure 1d). CellTrace staining revealed, though, that EGT inhibited $Foxp3^-$ $CD4^+$ and $CD8^+$ T cell proliferation (Figure 1e). T cell proliferation rapidly decreased at EGT concentrations higher than 25 uM (Figure S1b, Supporting Information).

This data indicates that sphingolipid metabolism affects T cell cultures. Sphingolipids are a major class of eukaryotic lipids that play critical roles in regulating cellular events such as apoptosis, cell growth and proliferation, signal transduction, and differentiation. Imbalances in sphingolipid levels can modulate T-cell function, contribute to chronic inflammation, and mediate TCR signaling.[13,21–23] EGT increased Foxp3 expression and T_{reg} cell frequency in CD4+ and CD8+ T cells, while simultaneously reducing T cell proliferation, with no observed cellular toxicity. However, these results were obtained using naïve T cells, leaving the effect of EGT on activated T cells unclear. This data also does not indicate whether the increased fractions of T_{regs} result from the enrichment of endogenous $Foxp3^+$ cells or the conversion of $T_{eff/em}$ cells into T_{regs}.

2.2. Eliglustat Inhibits $Foxp3^-$ T Cell Proliferation and Enriches T_{regs} in Originally $Foxp3^-CD4^+$ Populations

We next examined if the impact of EGT on the T cell population was due to differential effects on the proliferation rates of $Foxp3^-$ T and T_{reg} ($Foxp3^+$) cells. We isolated $CD4^+$ T cells from Foxp3-eGFP reporter mice and sorted them as $CD4^+eGFP^-$ ($Foxp3^-$) and $CD4^+eGFP^+$ ($Foxp3^+$, T_{reg}) cells. Each cell population was stimulated with anti-CD3/anti-CD28 beads, IL-2, in the presence or absence of EGT. While EGT significantly reduced the proliferation rate of $Foxp3^-$ cells, it had no significant effect on T_{reg} cell proliferation (**Figure 2**a). The capacity of EGT to generate T_{regs} from naïve $Foxp3^-$ T cells was next examined. Helper T cells were depleted of $CD4^+eGFP^+$ ($Foxp3^+$) T_{regs} and the remaining $CD4^+eGFP^-$ ($Foxp3^-$) cells were cultured in the presence or absence of EGT, with anti-CD3/anti-CD28 beads, and IL-2. The number of newly generated T_{regs} was evaluated after 72 h. EGT increased the number of $Foxp3^+$ cells from ≈2% in the untreated group to ≈12% after treatment (Figure 2b). To explore the role of TGF-β in EGT T_{reg} formation, T cell cultures were treated with an inhibitor of TGF-β receptor I. This resulted in a decrease in Foxp3-expressing T cells (Figure S4, Supporting Information). However, when compared to untreated controls, EGT treatment still led to a statistically-significant increase in the T_{reg} fraction, suggesting that endogenous TGF-β is not required for EGT-dependent Foxp3 induction in vitro. To test whether the EGT-induced T_{regs} were functional in suppressing T cell proliferation, T_{regs} from in vitro cultures treated with EGT or TGF-β were sorted and co-incubated with naive CellTracer-stained T cells, referred as the responder T cells, anti-CD3/CD28 mAb-coated beads, and IL-2. EGT-induced T_{regs} demonstrated similar suppressive activity to TGF-β-induced T_{regs} (Figure 2c), confirming that EGT-induced T cells not only expressed Foxp3 but also functioned as suppressive cells. To determine if EGT was able to induce Foxp3 expression not only in naïve T cells but also in activated T cells, $CD4^+$ T cells were first stimulated with anti-CD3/CD28 mAb-coated beads and IL-2 for 10 days. On day 10, 42% of the T cells were $CD44^+CD62L^-$, 57% $CD44^+CD62L^+$, and the remaining 1% was $CD44^-$ (Figure S5, Supporting Information). The cells were then treated with EGT or TGF-β for 72 h, and EGT exposure led to an increased percentage, MFI, and number of $Foxp3^+$ T cells (Figure 2d).

These findings indicate that in vitro T-cell activation in the presence of EGT elicits Foxp3 expression in naïve T cells. EGT differentially affected the proliferation of $CD4^+$ T cells, favoring the proliferation of T_{regs} that were functional immunosuppressors. The T_{reg}-promoting activity of EGT makes it a promising candidate for clinical applications as an immunosuppressant. While various factors, such as the mTOR inhibitor rapamycin, TGF-β, butyrate, and all-trans retinoic acid (ATRA), can induce T_{regs} from naïve T cells,[24] only one other drug has been reported to generate T_{reg} from $T_{eff/em}$ cells.[6] In accordance to previous literature, TGF-β–dependent generation of T_{regs} was only attainable from naïve T cells, and no Foxp3 induction was observed in activated $CD4^+$ cells exposed to TGF-β alone. We report that EGT was sufficient to induce Foxp3 in activated and differentiated T cells in vitro suggesting that it is a promising immunosuppressive drug that needs to be further studied. Other reported Foxp3-inducing substances, require exogenous TGF-β for T_{reg} cell induction. Blocking TGF-β receptor I elicited a decrease in Foxp3 expression suggesting that exogenous TGF-β is still involved in EGT-mediated immunosuppression. However, when compared to the control, EGT demonstrated a significant increase in T_{regs} suggesting that TGF-β is not strictly required for EGT T_{reg} induction and that other independent pathways might be involved.

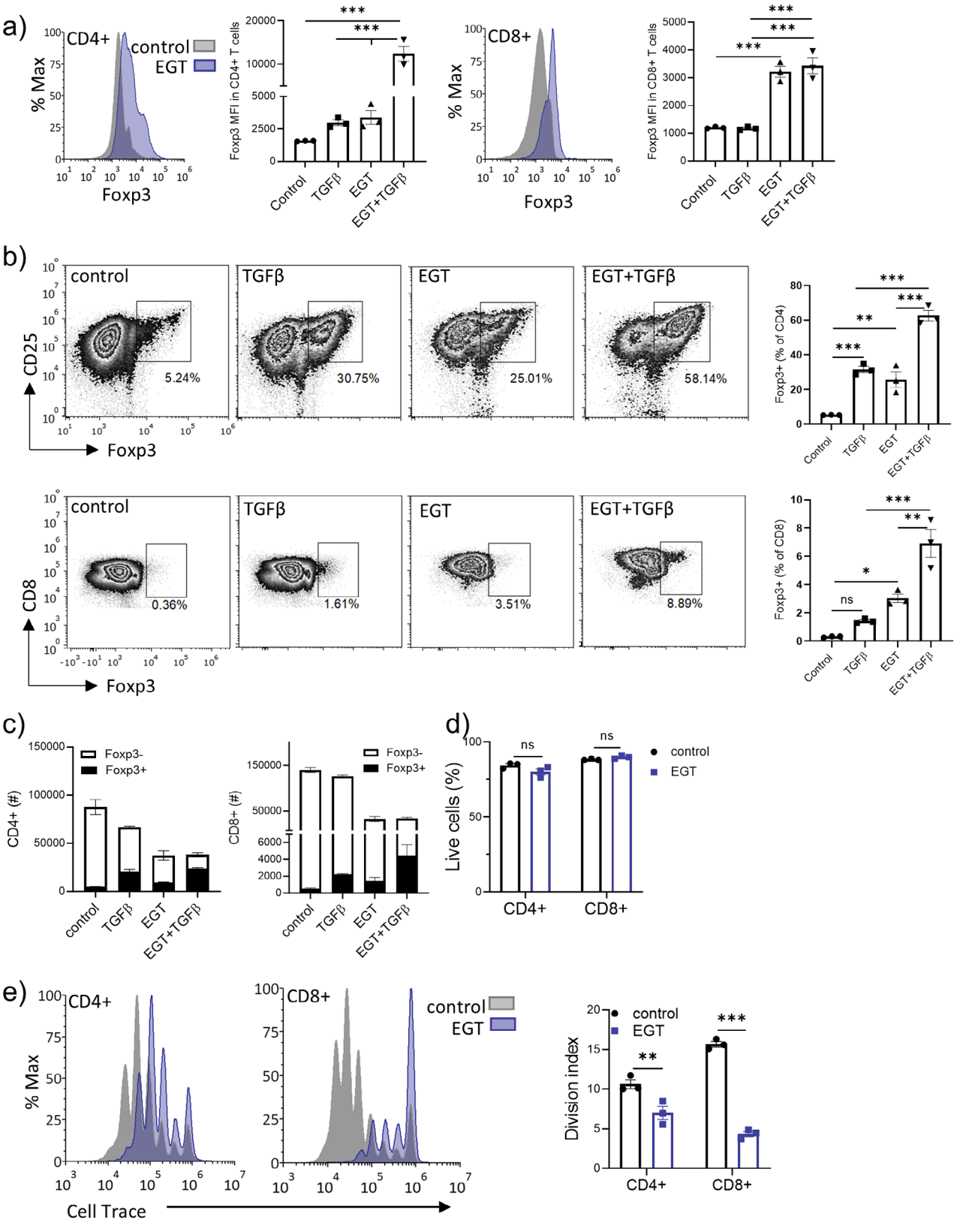

The exact mechanism by which glucosylceramide synthase inhibition results in increased Foxp3 expression remains to be fully understood, together with its effect on other T helper cell subsets. A possible mechanism might involve elevated levels of ceramide –the substrate of glucosylceramide synthase– blocking the PI3K-Akt-mTOR pathway and thereby inducing T_{regs}.[25,26] To better understand this effect, additional mechanistic experiments are required. Since the use of EGT is limited by its rapid clearance from the body, the risk of prolonging cardiac intervals, and poor penetration into the central nervous system[27] we next developed a biomaterial-based approach to enrich T_{regs} directly in vivo.

2.3. Biomaterial-Based Approach to Enhance T Cell Enrichment In Vivo

As the accumulation of T_{regs} in vivo has great potential for the treatment of autoimmune disorders and immunopathology, we designed a biomaterial to broadly enrich activated T cells locally, and subsequently accumulate T_{regs} via exposure to EGT (**Figure 3a**). This strategy would allow T_{reg} formation without the need of ex vivo expansion and manipulation, bypass the need of drugs that cross biological barriers, and reduce systemic off-target effects. Macroporous cryogels have already been implemented for drug delivery and as scaffolds for T cell delivery.[28–30] These materials can be fabricated by modifying alginate with tetrazine and type I collagen with norbornene (Figure 3b; Figure S8, Supporting Information). The extent of polymer functionalization was quantified via NMR and the degrees of functionalization were 1.5% and 2.1% for alginate–tetrazine (Figure S8, Supporting Information) and collagen–norbornene (Figures S9 and S10, Supporting Information), respectively. Tetrazine and norbornene undergo a bio-orthogonal inverse electron demand Diels–Alder click reaction upon mixing.[28] The reason for choosing tetrazine and norbornene ad click-reacting groups is due to its kinetics ($k_2 \approx 1.9 - 3.3\ M^{-1}s^{-1}$) which are fast enough to give a solid-like material on the experimental timescale yet allow sufficient time to cast the hydrogel before the crosslinking is completed.[31,32] Additionally, its biorthogonality makes it compatible with cellular environments and it has been widely used for the formation of alginate hydrogels with tunable mechanical properties by our group.[28,31,33,34] Under cryogelation conditions, this reaction produces macroporous cryogels with shape recovery properties, making them suitable for extruding them through needles.[28–30] After formation, cryogels were labeled with iFluor 488 by leveraging unreacted norbornene groups and imaged via confocal microscopy (Figure 3c). Cryogels exhibited a range of pore areas (Figure 3d; Figure S6, Supporting Information), with the average pore area and length ≈1100 μm^2 and 31 μm, respectively. Since the mean pore size is one order of magnitude larger than the diameter of T cells, cryogels were expected to allow cell trafficking.[35] When subjected to oscillatory shear, the formed cryogels exhibit a macroscopic elastic behavior over the frequency range of 0.01–100 rad s^{-1} (shear strain, γ = 1%, Figure 3e). The cryogels exhibited reproducible mechanical properties with a storage modulus of ≈380 ± 83 Pa, a loss modulus of 42 ± 12 Pa, and a loss factor of 0.11 ± 0.01 (oscillatory frequency, ω = 1 rad s^{-1} and γ = 1%, Figure 3f). When cryogels underwent oscillatory shear between 0.1 and 10% they maintained their solid-like properties (ω = 1 rad s^{-1}, Figure S11, Supporting Information).

Chemokines were incorporated into the cryogels to promote the active attraction and enrichment of activated T cells. C-X-C motif chemokine receptor 3 (CXCR3), a chemokine receptor that is highly expressed on T_{eff} cells, plays an important role in directing T cell trafficking. The CXCR3 ligands CXCL10 (interferon gamma-induced protein 10), and CXCL11 (interferon–inducible T Cell Alpha Chemoattractant) were loaded into cryogels in the absence or presence of laponite nanoparticles. Laponite particles are synthetic disk-shaped nanoclays that are commonly used in biomedical research thanks to their high surface area, and charge characteristics.[36] In aqueous media, they have a negatively charged face and a slightly positively charged edge. Laponite has been previously used to delay the release of molecules from scaffolds due to electrostatic interactions.[28,36,37] Since both CXCL10 and CXCL11 have an isoelectric point of ≈10, at physiological pH, these chemokines are positively charged and are adsorbed onto the surface of laponite particles (**Figure 4a**).[38] Loaded laponite particles are incorporated into cryogels by mixing them in the formulation prior to cryogelation and their impact on chemokine release properties tested (Figure 4b). CXCL10 and CXCL11 were both rapidly released from cryogels in the absence of laponite, but the release kinetics of both were significantly slowed in the presence of laponite (Figure 4c). For subsequent experiments, CXCL10 and CXCL11 were loaded into cryogels together with laponite to allow for a sustained chemokine release over several days. Blank, CXCL10-, or CXCL11-loaded cryogels were injected into subcutaneous tissue in the flank of mice to assess their capacity to increase T cell accumulation in situ. After two days, CXCL10 and CXCL11-loaded cryogels demonstrated a significantly higher $CD4^+$ and $CD8^+$ T cell infiltration when compared to blank cryogels (Figure 4d). Flow cytometry analysis showed that the majority of T cells in the scaffold displayed the phenotype of activated T cells ($CD44^{high}$) with the $CD4^+$ T cell subset largely expressing markers of effector/memory, $CD44^{high}$ $CD62L^{low}$, and the $CD8^+$ T cells primarily exhibiting markers of central memory,

Figure 1. Eliglustat is a Foxp3 inducer in naïve T cells. Naïve $CD4^+$ or $CD8^+$ T cells were isolated from the spleens of Foxp3-eGFP reporter mice. Cells were stimulated with anti-CD3/CD28 mAb-coated beads and IL-2 in the presence or absence of eliglustat (EGT, 10 μM) or TGF-β (0.5 ng mL^{-1}) for 72 h. a) In vitro induction of Foxp3 expression in EGT-treated mouse naïve $CD4^+$ T cells, and in $CD8^+$ T cells. Representative histograms of Foxp3 expression in $CD4^+$ and $CD8^+$ T cells and average mean fluorescence intensity (MFI) values of Foxp3. ($n = 3$). $^{***}p < 0.001$ by two-way ANOVA followed by Tukey's multiple comparison test. b) Representative Foxp3 staining and percentages of Foxp3+ cells among $CD4^+$ or $CD8^+$ T cells after respective stimulation are shown ($n = 3$). $^{*}p < 0.05$, $^{**}p < 0.01$, $^{***}p < 0.001$ by two-way ANOVA followed by Tukey's multiple comparison test. ns, not significant. c) Cell number of $Foxp3^+$ and $Foxp3^-$ cells among $CD4^+$ or $CD8^+$ T cells after respective stimulation ($n = 3$). Statistical analysis in Figure S1 (Supporting Information). d) $CD4^+$ or $CD8^+$ T Cell survival in the presence or absence of EGT (10 μM) for 24 h. ($n = 3$). Statistical analysis was performed using two-way ANOVA. ns, not significant. e) In vitro effects of EGT on the proliferative activity of naïve T cells. CellTrace Violet-labeled cells were stimulated with anti-CD3/CD28 Dynabeads in the presence or absence of EGT (10 μM) and analyzed by flow cytometry after 72 h. Representative histograms are shown ($n = 3$). $^{**}p < 0.01$, $^{***}p < 0.001$ by two-way ANOVA followed by Tukey's multiple comparison test.

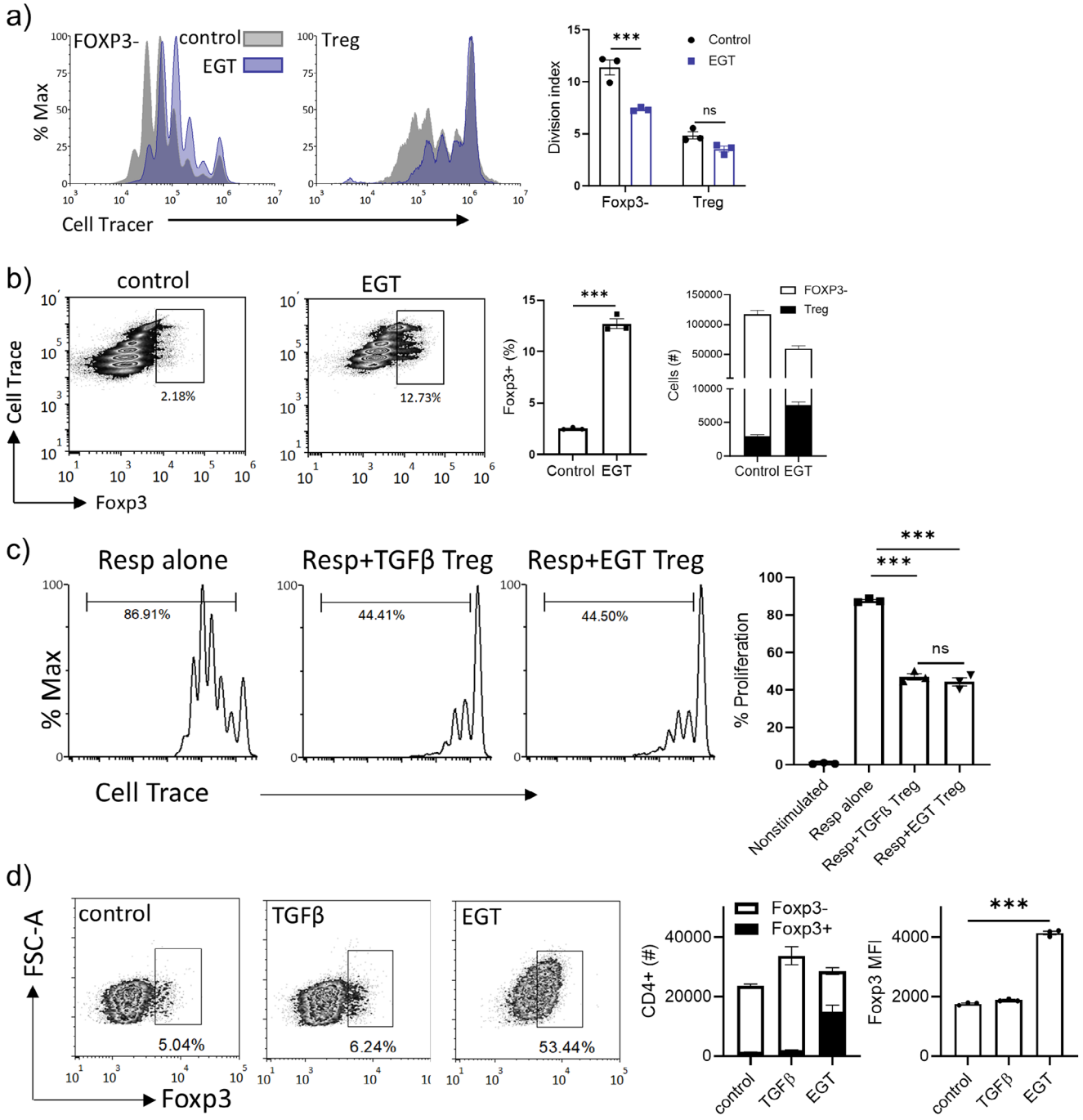

Figure 2. Eliglustat Inhibits T_{con} Cell Proliferation and Promotes T_{regs} formation. $CD4^+$ T cells were isolated from Foxp3-eGFP reporter mice and sorted as $CD4^+eGFP^-$ T_{con} and $CD4^+eGFP^+$ T_{regs}. After sorting, CellTrace Violet-labeled cells were stimulated with anti-CD3/CD28 Dynabeads in the presence or absence of EGT (10 μM) and analyzed by flow cytometry after 72 h (a, b). a) In vitro effects of EGT on the proliferative activity of T_{con} and T_{regs}. Representative histograms are shown ($n = 3$). $^{***}p < 0.001$ by two-way ANOVA followed by Tukey's multiple comparison test. ns, not significant. b) EGT promotes T_{reg} formation. $CD4^+eGFP^-$ were stimulated with anti-CD3/CD28 Dynabeads in the presence (EGT) or absence (control) of EGT (10 μM) and analyzed by flow cytometry after 72 h. Representative Foxp3 staining and percentages of $Foxp3^+$ cells are shown ($n = 3$). $^{***}p < 0.0001$ by unpaired, two-tailed *t*-test. c) In vitro suppression assay using in vitro TGF-β or EGT-induced T_{regs} ($n = 3$). T_{reg} versus responder T cell (Resp) ratio was 1:1. Vertical bars indicate means ± SEM. $^{***}p < 0.001$ by one-way ANOVA followed by Tukey's multiple comparison test. ns, not significant. d) In vitro induction of Foxp3 expression in EGT-treated mouse activated $CD4^+$ T cells. $CD4^+$ T Cells were stimulated with anti-CD3/CD28 mAb-coated beads and IL-2 for 10 days. At day 10, eliglustat (EGT, 10 μM) or TGF-β (0.5 ng mL^{-1}) was added to the media for 72 h. Representative Foxp3 staining, percentages of $Foxp3^+$ cells, cell number of $Foxp3^+$ and $Foxp3^-$ cells among $CD4^+$, and average mean fluorescence intensity (MFI) values of Foxp3 after respective stimulation are shown ($n = 3$). $^{***}p < 0.001$ by two-way ANOVA followed by Tukey's multiple comparison test. ns, not significant.

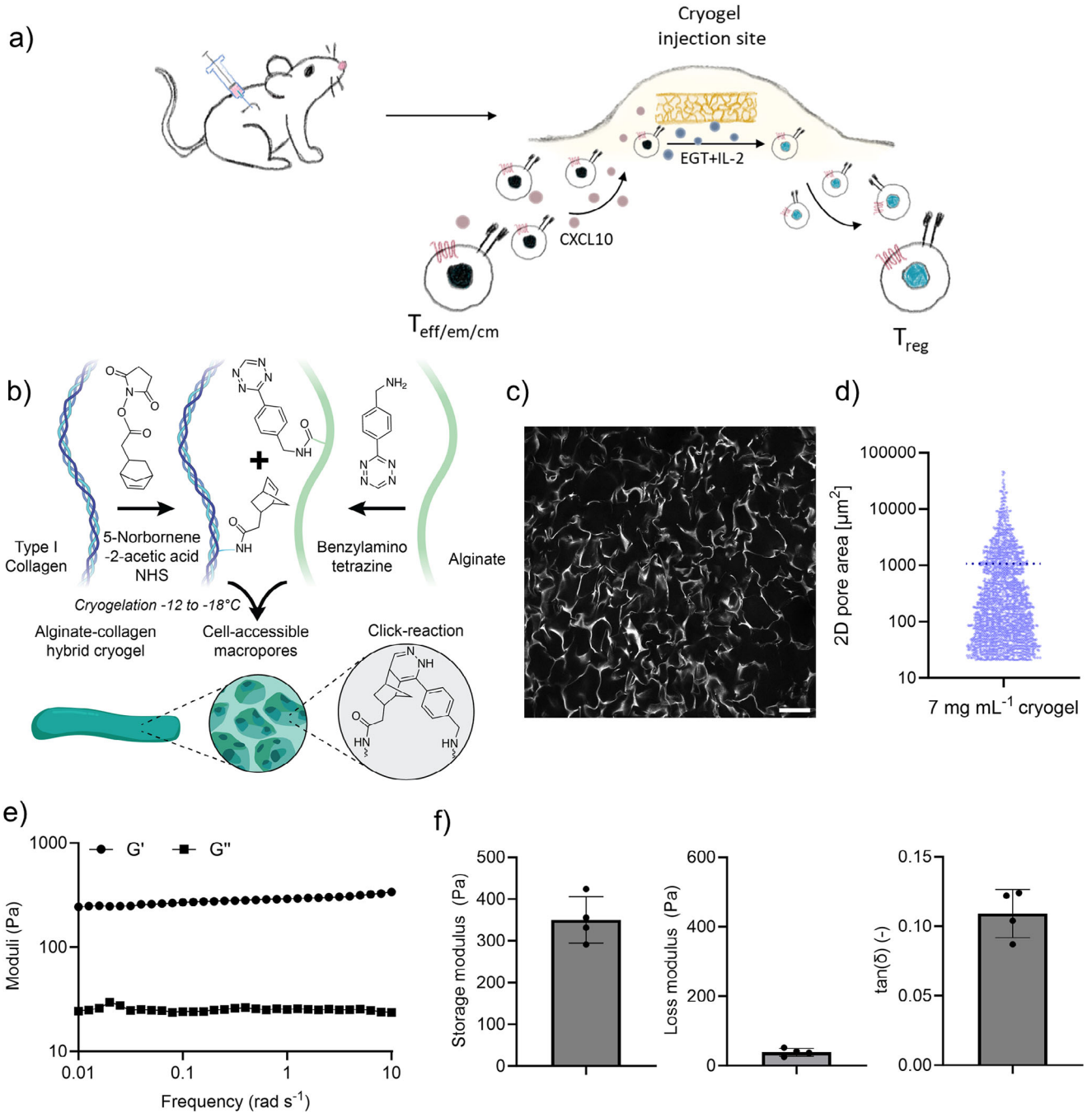

Figure 3. Strategy for recruiting T cells and accumulating T_{regs} in vivo a) A schematic illustration of the in situ recruitment and accumulation of activated T cells into Treg within cryogels. CXCR3 ligands (CXCL10/11) are released from cryogels to facilitate the migration of activated CXCR3+ $T_{eff/em/cm}$ cells to the gel scaffold. Within the scaffold, EGT and IL-2 are released, promoting T_{regs}, which can then exit the scaffold to induce immune suppression. b) Cryogel fabrication schematic: Type I collagen and alginate were respectively functionalized with norbornene and tetrazine. Cryogelation was performed at −12 to −18 °C to create macropores. c) Confocal image of a cryogel labeled with iFluor 488 demonstrating the pore architecture. Scale bar: 50 µm. D) 2D pore area distribution of 1774 pores measured from confocal images. Plot information: minimum = 21 µm², maximum = 45 866 µm², 25th percentile = 58 µm², median = 180 µm², 75th percentile = 836 µm², mean (dotted line) = 1077 µm², standard deviation = 3154 µm². e) Frequency sweep of cryogels at oscillatory strains of $\gamma = 1\%$ measured by shear rheology. Panel shows one representative curve ($n = 4$). f) Macroscopic storage and loss moduli, and loss factor of cryogels at $\gamma = 1\%$ and oscillatory frequency $\omega = 1$ rad s^{-1} ($n = 4$).

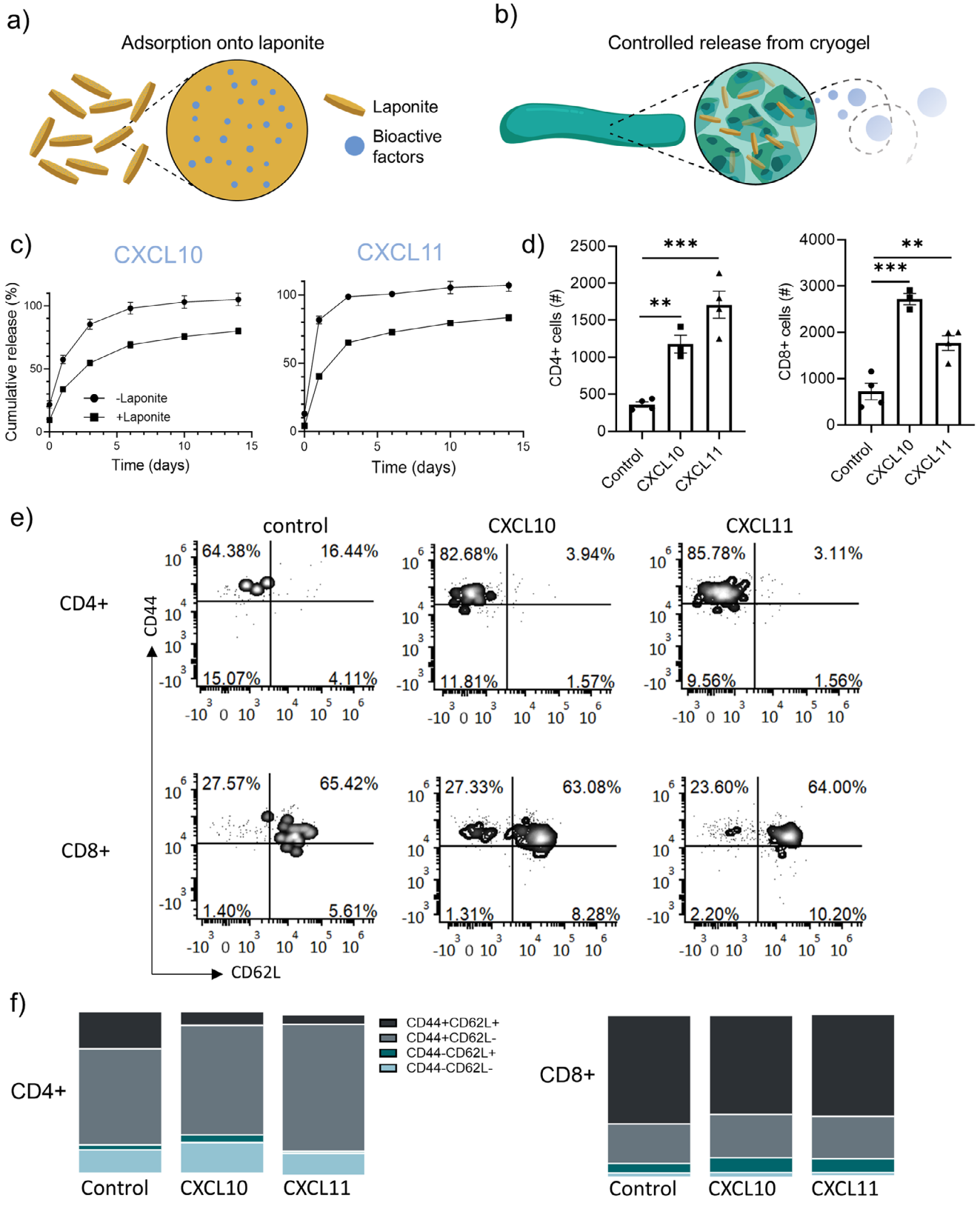

$CD44^{high}$ $CD62L^{high}$, (Figure 4e,f). Since CXCL10- and CXCL11-loaded cryogels exhibited similar results, for subsequent experiments, only CXCL10 was used.

Biomaterial scaffolds have been previously used to recruit various types of cells, including stem cells for tissue regenerative therapies,[39] dendritic cells as antigen-presenting cells for vaccines,[30] and – more recently – T cells for enhancing CAR-T cell therapy.[40,41] Our data provides a useful alternative strategy and demonstrates the ability to enhance the number of activated T cells by simply incorporating active enriching factors such as CXCL10 or CXCL11.

2.4. Biomaterial-Based T_{reg} Cell Accumulation In Vivo

The ability of cryogels to exhibit a sustained release of EGT and accumulate T_{regs} in vivo was assessed. Since IL-2 stimulates T cell expansion, it was included in the cryogel formulation to support T cells localizing to the injection site, analogous to its use in our in vitro studies. The formulation that was tested in vivo contained CXCL10 and IL-2, which were first independently complexed with laponite prior to cryogelation. EGT was included in the formulation as a soluble factor (**Figure 5a**). Analogously to CXCL10 and CXCL11, we examined the release properties of IL-2 after laponite complexation and found that most of the IL-2 is released over the first 3 days (Figure 5b). Dissolution of EGT in the polymers prior to cryogel formation resulted in a sustained release of EGT from cryogels over two days in vitro (Figure 5c). Cryogels were subcutaneously injected in mice to assess their capacity to promote T_{reg} cell enrichment in vivo. Cryogels were left blank, or loaded with a combination of CXCL10, IL-2-, and EGT. Cryogels have been widely utilized and have demonstrated good biocompatibility in vivo.[28–30] Upon loading with bioactive factors, all formulations were well tolerated and exhibited no observable effects on mouse behavior. After two days, cryogels loaded with both EGT and IL-2, and cryogels with all three factors had a significant increase in the percentage of T_{regs} (Figure 5d; Figure S13, Supporting Information). Cryogels containing only CXCL10 and EGT or CXCL10 and IL-2 did not show a notable increase in T_{reg} cell percentages, compared to blank cryogels. An increase in the ratio of $Foxp3^+$ T cells to other $CD4^+$ T cells was also found (Figure S14, Supporting Information). The inclusion of CXCL10 in the cryogels did not affect the percentage of T_{regs}, but did result in a higher total number of T_{regs} in the biomaterial niche (Figure 5e). The cryogel comprising CXCL10, EGT, and IL-2 was the only condition that exhibited a statistically-significant enrichment in T_{regs} number and percentage, and a higher CD4-to-CD8 ratio, indicating successful accumulation of T_{regs} in vivo. Immunohistochemistry and confocal imaging of cryogels loaded with CXCL10, EGT, and IL-2 confirmed the presence of $CD4^+$ T cells both inside the materials and in the proximal extracellular matrix (Figure 5f), with cells exhibiting $eGFP^+$ ($Foxp3^+$) as a confirmation for the presence of T_{regs}.

This biomaterial-based strategy for EGT delivery has the potential to address limitations of current eliglustat therapies. Currently, glucosylceramide synthase inhibitors are administered systemically, which can lead to suboptimal drug concentrations in target cells and increased risks of drug toxicity and non-specific effects. Despite the approval of EGT for Gaucher disease type 1, its application is hindered by its active metabolism via CYP2D6, its potential to prolong cardiac intervals, and its poor penetration into the central nervous system.[27] The biomaterial-based strategy employed here instead attracts activated T cells to the scaffold, where EGT is locally released to promote T_{reg} formation. This strategy of bringing target cells to the drug differs from conventional methods that deliver drug to the target tissue. We demonstrate that including CXCL10, EGT, and IL-2 in cryogels enriches the percentage and number of T_{regs} in vivo. In Gaucher disease mouse models, a safe and effective dose of EGT is 75 or 150 mg kg^{-1} day^{-1} administered for 10 weeks. In comparison, the typical daily dose for Gaucher disease patients is 168 mg day^{-1}, corresponding to ≈2.4–5 mg kg^{-1} day^{-1} based on an average adult weight of 70 kg. In this study, the 200 µg dose administered to an 8-week-old C57BL/6 mouse equates to roughly 8 mg kg^{-1}, but here delivered as a sustained-release formulation—indicating a lower effective dose than those used in conventional Gaucher Disease mouse models.[42] The impact of IL-2 likely relates to its critical roles in T_{reg} development and function.[43,44] More experiments are needed to investigate the exact mechanism of glucosylceramide synthase inhibitors as T_{reg} promoting therapies, and to apply these therapeutically. It has previously been demonstrated that polymer scaffolds loaded with antigen resulted in local accumulation of antigen-specific helper T cells,[45] and integrating that approach with our tolerogenic niche may enable enrichment of antigen-specific cells, resulting in a potent therapy against autoimmune diseases.

3. Conclusion

EGT was found to induce T_{regs} from both naïve and activated CD4+ T cells in vitro, suggesting that glucosylceramide synthase inhibitors may represent a broader new class of immunomodulatory drugs. Drugs targeting glucosylceramide synthase are currently used and being developed for treating Gaucher disease,

Figure 4. Recruitment of $T_{eff/em}$ Cells to Cryogel Loaded with CXCR3-Ligands a) Illustration showing the complexation of electrostatically-charged bioactive factors on laponite nanoparticles b) Loaded laponite nanoparticles were incorporated in cryogels by simply mixing them in the formulation prior to crosslinking. This led to delayed factor release. c) In vitro cumulative release of the CXCR3-ligands, CXCL10, and CXCL11 from cryogel scaffolds. 1 µg of recombinant protein in free form or adsorbed onto 1.5 µg of Laponite was included in 50 µL cryogels. The release assay was performed in 1% BSA in DPBS. The supernatants were harvested and the released factors were quantified by ELISA ($n = 3$). d–f) Mice were injected with cryogels loaded with either CXCL10 or CXCL11 and 1.5 µg of Laponite. Two days post cryogel injection, gels were harvested for T cells analysis. $n = 4$ (blank and CXCL11) or 3 (CXCL10) biologically independent animals per group. d) $CD4^+$ and $CD8^+$ cell numbers in cryogel scaffolds in vivo. Vertical bars indicate means ± SEM. $^{***}p < 0.001$, $^{**}p < 0.01$, by one-way ANOVA followed by Tukey's multiple comparison test. e) Representative flow cytometry plots of $CD4^+$ and $CD8^+$ T cell isolated from gels, stained to identify expression of markers typically utilized to identify effector/memory T cell phenotypes. f) Fraction of phenotypically naïve ($CD44^{low}$ $CD62L^{high}$), effector/memory ($CD44^{high}$ $CD62L^{low}$), central memory T cells ($CD44^{high}$ $CD62L^{high}$), and $CD44^{low}$ $CD62L^{low}$ of $CD4^+$ and $CD8^+$ T cells in the cryogels.

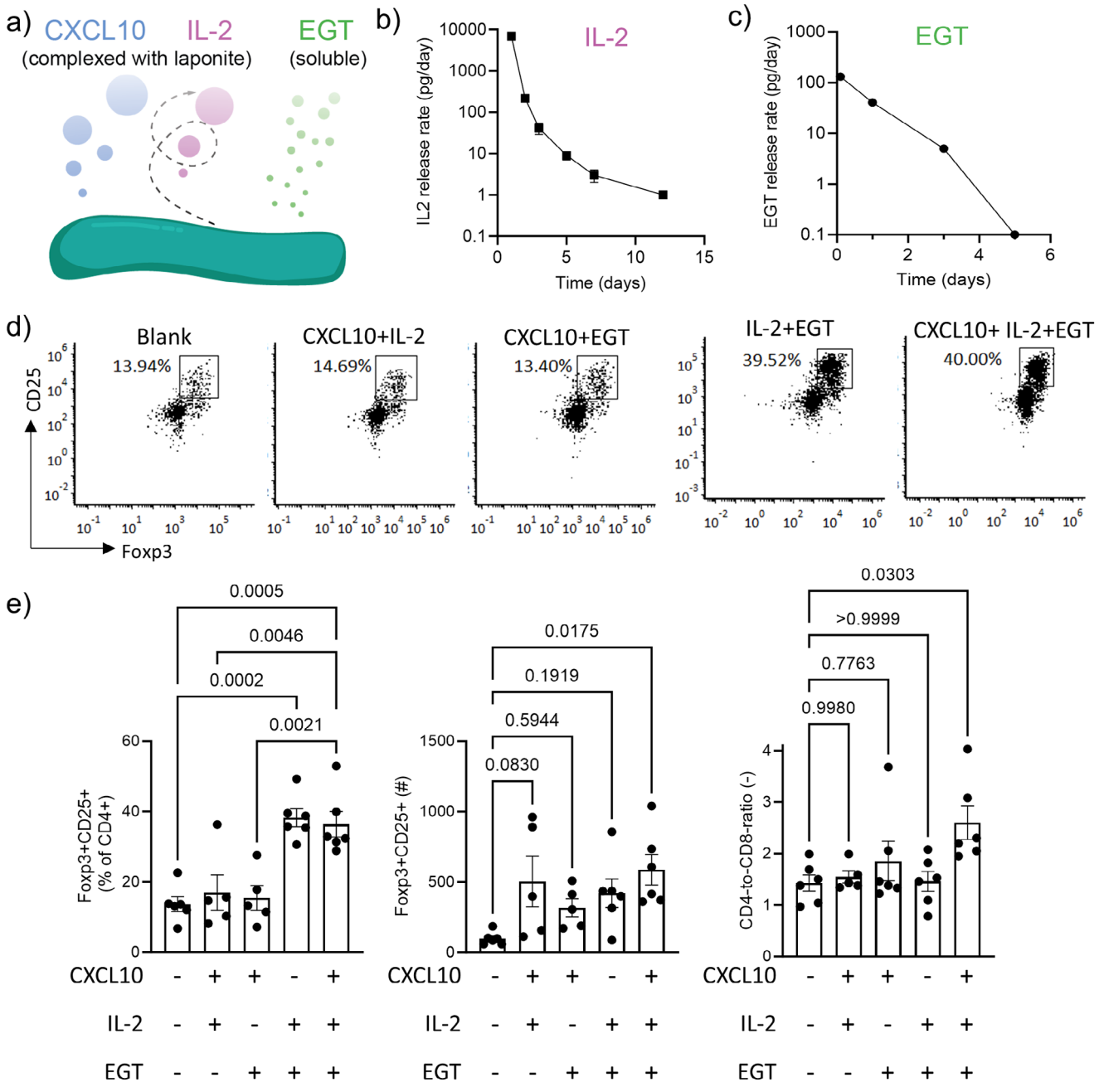

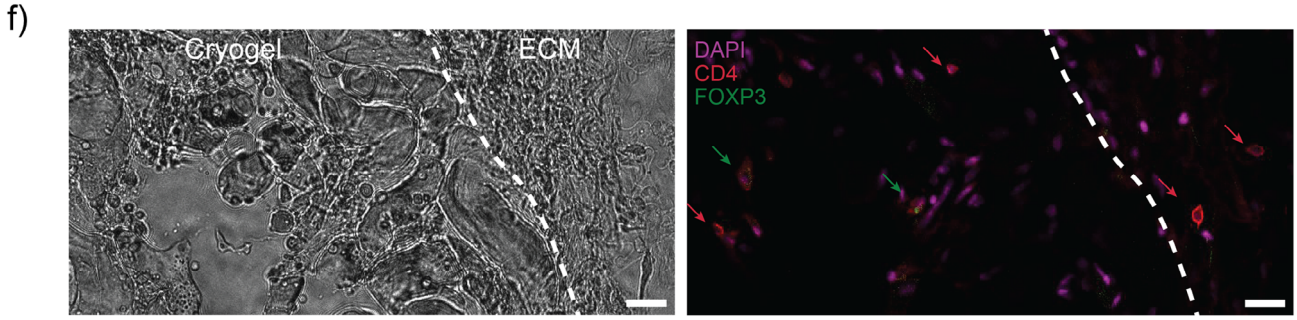

with the potential to be rapidly repurposed as immunosuppressants. $T_{eff/em}$ cells were enriched in a cryogel scaffold in vivo via sustained release of CXCL10, and cryogels delivering a combination of CXCL10, IL-2, and EGT led to increased numbers and percentages of T_{regs}. These results open new avenues for utilizing glucosylceramide synthase inhibitors in the treatment of inflammatory and autoimmune diseases, using biomaterial-based strategies in a variety of scenarios where T_{reg} cell enrichment is desirable.

4. Experimental Section

Mice: C57BL/6 (#000664), and Foxp3–enhanced green fluorescent protein (eGFP) reporter mice (#006772) were purchased from The Jackson Laboratory. All procedures were in accordance with the National Institutes of Health Guide for the Care and Use of Laboratory Animals and approved by the Harvard University Faculty of Arts and Sciences Institutional Animal Care and Use Committee (IACUC, protocol: 24-16-4).

T Cell Isolation, Culture, and Activation: $CD4^+$ or $CD8^+$ T cells were freshly isolated from mouse spleens using the naïve CD4+ or CD8α+ T Cell Isolation Kit that was magnetic-bead-based (Miltenyi # 130-104-453 or130-104-075). The manufacturer's protocol was followed. T cells were cultured in RPMI 1640 containing L-Glutamine supplemented with 10% heat-inactivated fetal bovine serum (Gibco #10-082-147), 1% penicillin/streptomycin, 25 mM 4-(2-hydroxyethyl)-1-piperazineethanesulfonic acid (HEPES, Gibco, #22400121), 55 µM β-mercaptoethanol, 1% of 100x non-essential amino acid (Lonza #13-144E), 100 mM sodium pyruvate (Lonza #13-115E), and 50 U mL^{-1} recombinant mouse IL-2 (BioLegend #575404). To activate T cells, Dynabeads Mouse T-Activator CD3/CD28 (ThermoFisher Scientific # 11452D) were used at a Dynabead to T cell ratio of 1:1. Some experimental conditions were treated with 10uM eliglustat hemitartrate (Selleck, #S4433) or 0.5 ng mL^{-1} TGF-β (PeproTech #100-21) by directly adding the compounds to the cell culture medium. In experiments where T cells were maintained for more than three days, fresh T cell medium supplemented with IL-2 was added every two days after day 3 in culture, and the cells were split to maintain a density of 5×10^5 cells mL^{-1}.

Materials Synthesis–Materials Synthesis–Alginate Chemical Functionalization: Carbodiimide chemistry was used to functionalize alginate with (4-(1,2,4,5-tetrazin-3-yl) phenyl methanamine hydrochloride (Karebay Biochem). Pronova ultrapure MVG sodium alginate was purchased from Novamatrix (guluronic acid to mannuronic acid ratio $\geq$ 1.5, viscosity > 200 mPa s at 1% in 20 °C water). Alginate was dissolved at 5 mg mL^{-1} in a pH 6.5 solution containing 0.1 M 2-(N-morpholino) ethanesulfonic acid (MES) and 0.3 M NaCl. For each gram of alginate, 1.9 g of ethyl-3-(3-dimethylaminopropyl)-carbodiimide hydrochloride (EDC) (ThermoFisher #22980), and 1.2 g of N-hydroxysuccinimide (NHS) (ThermoFisher #24500) were added to the solution. Under continuous stirring, 0.1 g of tetrazine was added, and the reaction was carried out overnight at room temperature. The product, tetrazine-modified alginate, was purified using a tangential flow filtration device (KrosFlow KR2i; Spectrum Labs) and a 1 kDa MWCO membrane. A 150 to 0 mM decreasing NaCl gradient was used. The solution was treated with 1 g activated charcoal, filtered through a 0.22-µm filter, and lyophilized.

Collagen Chemical Functionalization: Collagen was functionalized with norbornene using a previously published protocol.[28] A 5-Norbornene-2-acetic acid succinimidyl ester (Nb-NHS) (Sigma–Aldrich #776173) to Rat Tail Collagen Type I (Corning #354236 ratio of 1g: 10 g was used. Sodium hydroxide was used to neutralize collagen to pH 7.2–7.5. The solution was buffered with 10x DPBS, and diluted to a collagen concentration of 2 mg mL^{-1}. A solution of 2 mg mL^{-1} Nb-NHS in DMSO was prepared and diluted 10-fold in 1x PBS. Under continuous stirring, an equal volume of Nb-NHS was added to the collagen solution. The resulting final collagen concentration was of 1 mg mL^{-1}. The solution was kept at 4 °C for 5 h to delay collagen gelation. The reaction was quenched with 0.1 M acetic acid to re-acidify the collagen solution. The product, norbornene-modified collagen, was purified via dialysis against 0.025 M acetic acid for 4 days, filtration through 0.45 µm filters, and lyophilization.

4.0.0.1. Nuclear Magnetic Resonance Spectroscopy: ^1H nuclear magnetic resonance spectroscopy (Bruker AVANCE NEO 400, 400 MHz) was used to quantify the degree of substitution of collagen–norbornene or alginate–tetrazine. The alginate was dissolved in deuterium oxide with potassium hydrogen phthalate as internal standard. Collagen was dissolved in deuterated DMSO with tetramethylsilane as internal standard.[46] The specific details on the estimation of the degree of substitution are provided in the NMR figure captions (Figures S8–S10, Supporting Information).

Gel Permeation Chromatography: The molecular weight and dispersity of alginate–tetrazine was analyzed using gel permeation chromatography (1260 Infinity II GPC). 1 mg mL^{-1} polymer samples were dissolved in the mobile phase of DMF and filtered through 0.2 µm PTFE syringe filters. Molecular weight characteristics were evaluated against a calibration standard using a mobile phase flow rate of 0.5 mL min^{-1}.

Cryogel Fabrication: 0.8 wt.% vol^{-1} alginate–collagen cryogels were fabricated using a weight fraction of 60% alginate and 40% collagen. At least 48 h prior to cryogel fabrication, collagen-norbornene was dissolved at 4 °C to 9 mg mL^{-1} in 0.025 N acetic acid. On the day of cryogel fabrication. alginate tetrazine was dissolved to 2% wt vol^{-1} in water and the solution was cooled down to 4 °C. For cryogelation, the prepared collagen-norbornene was dissolved in cold 1 N NaOH, subsequently buffered with cold 10x DPBS and balanced with cold water. Alginate tetrazine was added to the solution, so the final concentrations of collagen and alginate were resepectively 3 and 4.5 mg mL^{-1}. To mold the cryogel, the prepared mixture was rapidly pipetted into a plastic tube (Tygon S3 E-3603, Grainger # ACF00004) and kept overnight at −15 °C in a freezer for cryopolymerization. Subsequently, the tube containing cryogels was thawed at room temperature, cut in ≈ 1 cm pieces that contain ≈50 µL of cryogel solution, and ejected by flushing the tubing with a minimal volume of PBS. To load bioactive molecules, a solution containing factors such as CXCL10, CXCL11, IL-2 and or eliglustat hemitartrate (5 µg) was prepared and included in the mixture before cryogelation. The release of recombinant murine IP-10 (CXCL10) (Peprotech #250-16), recombinant murine I-TAC (CXCL11) (Peprotech #250-29), or recombinant mouse IL-2 (Biolegend #575408) was delayed via complexation with laponite XLG (BYK additives). 1 mg mL^{-1} laponite was dissolved in milliQ water by vortexing extensively until the suspension became entirely clear. To adsorb bioactive factors, IL-2 (10000 IU) or CXCL10/11 (5 µg per 50 µL gel solution) were

Figure 5. Accumulation of T_{regs} in vivo a) Illustration showing the cryogel formulation used in the in vivo experiments — CXCL10 and IL-2 were complexed with laponite prior to cryogelation, whereas EGT was included as a soluble factor. b) Release of 10 ng IL-2 from 50 µL cryogels incubated in cell culture medium. The release supernatants were harvested periodically, and IL-2 was quantified by ELISA (n = 3). c) Release of eliglustat from cryogels. Eliglustat (200 µg) was incorporated in each 50 µL gel and incubated in DPBS. The release supernatants were harvested, and eliglustat was quantified by LCMS (n = 4, see Figure S12, Supporting Information to appreciate error bars in data). d–f) Mice were injected with cryogels loaded with combinations of CXCL10, IL-2, and eliglustat (EGT), as indicated. Gels were harvested 2 days post-cryogel injection for T_{reg} cell analysis. d) Representative T_{reg} cell staining ($CD4^+Foxp3^+CD25^+$) is shown (n = 3). e) Total number and percent of T_{reg} ($CD4^+Foxp3^+CD25^+$) of $CD4^+$ T cells as well as $CD4^+$-to-$CD8^+$ T cell ratio in the cryogels. n = 5–6 biologically independent animals per group. Vertical bars indicate means ± SEM. p-value was calculated by one-way ANOVA followed by Tukey's multiple comparison test. f) Phase contrast image (left), and immunohistochemistry (right) of cryogels harvested after 2 days post-injection in Foxp3-eGFP reporter mice. Nuclei are shown in magenta, $CD4^+$ T cells in red, and Foxp3-eGFP expression in green. Red arrows point to $CD4^+Foxp3^-$ T cells, whereas green arrows to $CD4^+Foxp3^-$ T cells.

incubated for 1 h at 4 °C with 1 or 1.5 µg of laponite, respectively. The bioactive factors and laponite were included in the cryogel mixture rior to cryogelation. The addition of laponite to IL-2 was performed according to previously published data.[37]

Cryogel Pore Size Quantification: After formation, cryogels were incubated with iFluor 488 tetrazine (AAT Bioquest #1014) solution (1:1000 in PBS) for 1 h at room temperature for labeling by leveraging unreacted norbornene functional groups. The staining solution was removed, the cryogels were washed three times with 1 mL PBS and imaged with Leica STELLARIS inverted confocal microscope at 20x magnification at $\lambda_{ex} = 491$ nm and $\lambda_{em} = 516$ nm. Images were taken every 20 µm in different sections of the cryogels. The pore area was quantified using a MATLAB code (Figure S4, Supporting Information) developed in-house by converting the pixel area into μm^2. Pore length was reported as the square root of the measured pore area.

Cryogel Rheological Characterization: The rheological properties of cryogels were measured with a stress-controlled rheometer (DHR-3, TA Instruments, New Castle, DE, USA) equipped with a 8 mm parallel plate geometry. All measurements were performed at 25 °C after an equilibration phase of 2 min. Glass slides were treated with Sigmacote to decrease cryogel adhesion during the cryogelation process. Disk-shaped cryogels were casted overnight between two evenly-spaced glass slides. Cryogels were thawed and, if their diameter exceeded 8 mm, they were trimmed using an 8 mm biopsy punch. Rigth after thawing, the materials were placed on the rheometer and the geometry was lowered by 50 um steps while monitoring the measured normal stress until contact was registered. This usually happened at 900 um, which was the gap size chosen for the measurements. Oscillatory frequency sweeps were carried out in the linear viscoelastic region at 1% strain.

Release of Bioactive Factors From Cryogels: Cryogels loaded with CXCL10, CXCL11, or eliglustat hemitartrate were incubated in 500 µL RPMI (CXCL10, CXCL11) or in PBS (EGT) at 37 °C. At selected time points, the release supernatant was retrieved for measurement and replaced by the same volume of fresh release medium. CXCL10, CXCL11 were quantified via ELISA (Thermo #BMS6018, EMCXCL11). To characterize the release of IL-2, 10 ng of IL-2 were adsorbed onto 1 ug of laponite and incorporated into the cryogels. The release assay was performed in 1 mL RPMI without phenol red supplemented with 1% penicillin/streptomycin and 20% FBS. At each timepoint the entire release supernatant was exchanged with fresh one and the concentration of IL-2 was quantified with an ELISA kit by following the manufacturer's instructions (ELISA MAX Standard Set Mouse IL-2, Biolegend). The released eliglustat hemitartrate was quantified via liquid chromatography–mass spectrometry (Agilent LC/MSD XT with Agilent 1260 Infinity II; SIM mode). 200 µL of the release supernatant was frozen, lyophilized, and dissolved in HPLC-grade acetonitrile. Insoluble components were spun down and the supernatant was filtered through 0.2 µL PTFE syringe filters. 3 µL of sample was separated by a C18 column (Agilent Poroshell 120, EC-C18, 1.9um, 2.1×50) using a gradient of acetonitrile and formic acid. The sample concentration was calculated by comparing with calibration curves of known samples.

Animal Studies: Cryogels were fabricated as described above and suspended in 0.2 mL of PBS. They were then syringe-injected through a 16G needle, with one cryogel subcutaneously injected per mouse. Cryogels processing: Harvested cryogels were transferred into gentleMacs C tubes (Miltenyi #130-093-237) with digestion media composed of RPMI 1640 supplemented with 10% FBS, 150U mL^{-1} collagenase type IV (Thermo #17104019), and 0.1 µg μL^{-1} DNAse 1 (Sigma #11 284 932 001). The cryogels were subjected to mechanical dissociation using the gentleMacs tissue dissociator (Miltenyi #130-093-235), followed by incubation at 37 °C for 25 min. A second round of mechanical dissociation was performed with the same dissociation protocol, after which the samples were incubated for an additional 15 min. To stop the enzymatic activity, MACS buffer (DPBS containing 0.5% BSA and 2 mM EDTA) was added, and the resulting solution was passed through a 30-µm strainer (Miltenyi #130-098-458).

Flow Cytometry–Surface Marker Staining: For the entire immunostaining protocol, cells were maintained at 4 °C. Cells were incubated with LIVE/DEAD Fixable Blue Dead Cell Stain (ThermoFisher Scientific #L23105) for 30 min at a 1:1000 dilution in PBS. The staining process was stopped using flow cytometry staining (FACs) buffer composed of 1% bovine serum albumin in PBS and 2 mM EDTA. To prevent non-specific binding, cells were treated with TruStain FcX Fc receptor blocking solution (BioLegend #101 319) for 5 min. Subsequently, a cocktail containing surface protein antibodies at a 1:50 dilution was added for 20 min. After staining, the cells were washed three times with FACs buffer. Data acquisition was performed using a Cytek Aurora Spectral Analyzer. For multi-parameter flow cytometry compensation, single-color compensation beads (Thermo #01-2222-41) were utilized. Gating strategies relied on fluorescence-minus-one (FMO) controls. A detailed list of antibodies used for flow cytometry is provided in Table S1 (Supporting Information).

Transcription Factor Staining: To stain for the transcription factor Foxp3, cells were fixed and then permeabilized utilizing the True-Nuclear Transcription Factor Buffer Set (BioLegend #424401) following the manufacturer's instructions. Foxp3 staining was performed at room temperature for 30 min. Subsequently, the cells were washed and analyzed using the Cytek Aurora Spectral Analyzer.

Flow Cytometry Analyses: FCS files were analyzed with FCS Express 7 using the following hierarchy: SSC-A/FSC-A to gate for events to analyze → FSC-H/FSC-A to gate for single cells → FSC-H/Live and Dead to gate for live cells → FSC-H/CD45 to gate for immune cells → TCRβ/CD3 to gate for T cells → CD4/CD8 to gate for $CD4^+$ or $CD8^+$ T cells. Gates downstream of $CD4^+$ and $CD8^+$ T cells are performed using FMO controls or compensated single-cells. Flow cytometry intensity values are exported as Excel files for unsupervised analyses. A representative gating strategy is shown in Figure S3 (Supporting Information).

Immunohistochemistry: Cryogels were excised together with the skin and fixed for 1 h in 4% PFA at 4 °C. The samples were washed in PBS and preserverd in 30% sucrose overnight at 4 °C, and then frozen in OCT solution. Tissues were cryosectioned with a Leica CM3050 S cryostat into 30 – 50 µm slices, mounted on Superfrost Plus slides, and preserved at −20 °C. For immunostaining, the area of the sectioned samples was delimited with and ImmEdge Pen (Vector Laboratories). The samples were washed 3 times with PBS and blocked with a 5% solution of 1:1 BSA and horse serum for 30 min. The primary antibody, anti-mouse CD4 (Biolegend, Clone: RM4-5, Isotype: Rat IgG2a, Cat#:100505), was diluted 1:100 in blocking buffer and added to the specimen for 1 h at room temperature. After 3 washes with blocking buffer, the samples were incubated with the secondary antibody, goat anti-rat AlexaFluor 594 (Invitrogen, Cat#:A-11007) at a dilution of 1:500. The samples were washed three times with blocking buffer, stained with 0.5 µg mL^{-1} DAPI in PBS and washed with PBS and with blocking buffer once. ProLong Gold Antifade Mountant (Thermo Fisher) was added, the specimen were and covered with a cover slip, and imaged with a Leica STELLARIS inverted confocal microscope with a 25x water immersion objective. Images were analyzed with ImageJ (1.54p).

Statistical Analysis: The statistical analyses were performed using GraphPad Prism as detailed in the figure legends.

Supporting Information

Supporting Information is available from the Wiley Online Library or from the author.

Acknowledgements

The authors acknowledge Z. Niziolek at the Bauer Core Facility at Harvard for help with flow cytometry. This work was supported by the National Institutes of Health (R01 CA276459), and the Wyss Institute. The work of G.B. was supported by the Swiss National Science Foundation via a Postdoc Mobility grant (P500PN_210721). The work of W.J. was supported by the National Cancer Institute (K00 CA253759). The work of Y.B. was supported by a T-32 NIH grant.

Conflict of Interest

E.B.V. and D.J.M. have filed a patent application on the technology described in this manuscript.

Author Contributions

E.B.V. and D.M. designed the study. E.B.V. and G.B. performed experiments, analyzed data, and produced the figures. H.H., M.T.D., Y.B., W.J., K.A., and M.S. performed experiments. E.B.V., G.B., and D.M. wrote the manuscript. All authors critically revised the manuscript before publication.

Data Availability Statement

The data that support the findings of this study are available from the corresponding author upon reasonable request.

Keywords

glucosylceramide synthase inhibitor, hydrogel, regulatory T cells, sphingolipids, sustained release

Received: March 22, 2025
Revised: May 26, 2025
Published online:

[1] R. Pahwa, A. Goyal, I. Jialal, in StatPearls., StatPearls Publishing Copyright 2023, StatPearls Publishing LLC, Treasure Island (FL) **2023**, ineligible companies.
[2] C. Selck, M. Dominguez-Villar, *Front Immunol* **2021**, *12*, 661875.
[3] M. Miyara, Y. Ito, S. Sakaguchi, *Nat Rev Rheumatol* **2014**, *10*, 543.
[4] C. Raffin, L. T. Vo, J. A. Bluestone, *Nat. Rev. Immunol.* **2020**, *20*, 158.
[5] M. Kanamori, H. Nakatsukasa, M. Okada, Q. Lu, A. Yoshimura, *Trends Immunol.* **2016**, *37*, 803.
[6] M. Akamatsu, N. Mikami, N. Ohkura, R. Kawakami, Y. Kitagawa, A. Sugimoto, K. Hirota, N. Nakamura, S. Ujihara, T. Kurosaki, H. Hamaguchi, H. Harada, G. Xia, Y. Morita, I. Aramori, S. Narumiya, S. Sakaguchi, *Science Immunology* **2019**, *4*, aaw2707.
[7] L. M. Casey, J. T. Decker, J. R. Podojil, L. Rad, K. R. Hughes, J. A. Rose, R. M. Pearson, S. D. Miller, L. D. Shea, *Biotechnol. Bioeng.* **2023**, *120*, 284.
[8] M. A. Thelin, S. Kissler, F. Vigneault, et al., In *Vivo Enrichment of Diabetogenic T Cells. Diabetes.*, **2017**, *66*, 2220.
[9] K. Adu-Berchie, D. J. Mooney, *Acc. Chem. Res.* **2020**, *53*, 1749.
[10] J. G. Graham, X. Zhang, A. Goodman, K. Pothoven, J. Houlihan, S. Wang, R. M. Gower, X. Luo, L. D. Shea, *Tissue Eng Part A* **2013**, *19*, 1465.
[11] C. S. Verbeke, D. J. Mooney, *Adv. Healthcare Mater.* **2015**, *4*, 2677.
[12] C. S. Verbeke, S. Gordo, D. A. Schubert, S. A. Lewin, R. M. Desai, J. Dobbins, K. W. Wucherpfennig, D. J. Mooney, *Adv. Healthcare Mater.* **2017**, *6*, 1600773.
[13] J. C. Hartel, N. Merz, S. Grösch, *Front. Pharmacol.* **2022**, *13*, 1002915.
[14] M. Maceyka, S. Spiegel, *Nature* **2014**, *510*, 58.
[15] T. Zhang, A. A. de Waard, M. Wuhrer, R. M. Spaapen, et al., *Front Immunol* **2019**, *10*, 90.
[16] L. Martin-Gutierrez, K. E. Waddington, A. Maggio, L. Coelewij, A. E. Oppong, N. Yang, M. Adriani, P. Nytrova, R. Farrell, I. Pineda-Torra, E. C. Jury, *Clin. Exp. Immunol.* **2024**, *217*, 204.
[17] Y. Zhu, N. Gumlaw, J. Karman, H. Zhao, J. Zhang, J.i-L. Jiang, P. Maniatis, A. Edling, W.-L. Chuang, C. Siegel, J. A. Shayman, J. Kaplan, C. Jiang, S. H. Cheng, *J. Biol. Chem.* **2011**, *286*, 14787.
[18] T. Kanno, R. Konno, M. Sato, A. Kurabayashi, K. Miyako, T. Nakajima, S. Yokoyama, S. Sasamoto, H. K. Asou, J. Ohzeki, Y. Hasegawa, K. Ikeda, Y. Kawashima, O. Ohara, Y. Endo, *Commun. Biol.* **2024**, *7*, 622.
[19] F. M. Platt, A. d'Azzo, B. L. Davidson, E. F. Neufeld, C. J. Tifft, *Nat. Rev. Dis. Primers* **2018**, *4*, 27.
[20] T. M. Cox, J. Charrow, E. Lukina, P. K. Mistry, M. C. Foster, M. J. Peterschmitt, *Genet Med* **2023**, *25*, 100329.
[21] G. McDonald, S. Deepak, L. Miguel, C. J. Hall, D. A. Isenberg, A. I. Magee, T. Butters, E. C. Jury, *J. Clin. Invest.* **2014**, *124*, 712.
[22] Y. A. Hannun, L. M. Obeid, *Nat. Rev. Mol. Cell Biol.* **2018**, *19*, 175.
[23] M. Lee, S. Y. Lee, Y.-S. Bae, *Exp. Mol. Med.* **2023**, *55*, 1110.
[24] A. Schmidt, M. Eriksson, M. M. Shang, H. Weyd, J. Tegnér, et al., *Plos One* **2016**, *11*, 0148474.
[25] P. Hartwig, D. Höglinger, *Int. J. Mol. Sci.* **2021**, *22*, 7065.
[26] D. Valmori, V. Tosello, N. E. Souleimanian, E. Godefroy, L. Scotto, Y.u Wang, M. Ayyoub, *J. Immunol.* **2006**, *177*, 944.
[27] J. A. Shayman, V. Hinkovska-Galcheva, L. Shu, *Methods Mol Biol* **2023**, *2613*, 271.
[28] K. Adu-Berchie, J. M. Brockman, Y. Liu, T. W. To, D. K. Y. Zhang, A. J. Najibi, Y. Binenbaum, A. Stafford, N. Dimitrakakis, M. C. Sobral, M. O. Dellacherie, D. J. Mooney, *Nat. Commun.* **2023**, *14*, 3546.
[29] S. A. Bencherif, R. W. Sands, D. Bhatta, P. Arany, C. S. Verbeke, D. A. Edwards, D. J. Mooney, *Proc Natl Acad Sci U S A* **2012**, *109*, 19590.
[30] S. A. Bencherif, R. Warren Sands, O. A. Ali, W. A. Li, S. A. Lewin, T. M. Braschler, T.-Y.u Shih, C. S. Verbeke, D. Bhatta, G. Dranoff, D. J. Mooney, *Nat. Commun.* **2015**, *6*, 7556.
[31] R. M. Desai, S. T. Koshy, S. A. Hilderbrand, D. J. Mooney, N. S. Joshi, *Biomaterials* **2015**, *50*, 30.
[32] Y. Deng, A. Shavandi, O. V. Okoro, L. Nie, *Carbohydr. Polym.* **2021**, *270*, 118360.
[33] K. H. Vining, A. Stafford, D. J. Mooney, *Biomaterials* **2019**, *188*, 187.
[34] H. Y. Yoon, D. Lee, D. K. Lim, H. Koo, K. Kim, et al., *Adv. Mater.* **2022**, *34*, 2107192.
[35] R. Hallmann, X. Zhang, J. Di Russo, L. Li, J. Song, M.-J. Hannocks, L. Sorokin, *Curr. Opin. Cell Biol.* **2015**, *36*, 54.
[36] G. Kiaee, N. Dimitrakakis, S. Sharifzadeh, H.-J. Kim, R. K. Avery, K. M. Moghaddam, R. Haghniaz, E. P. Yalcintas, N. R. D.e Barros, S. Karamikamkar, A. Libanori, A. Khademhosseini, P. Khoshakhlagh, *Adv. Healthcare Mater.* **2022**, *11*, 2102054.
[37] S. T. Koshy, D. K. Y. Zhang, J. M. Grolman, A. G. Stafford, D. J. Mooney, *Acta Biomater.* **2018**, *65*, 36.
[38] Available from: http://isoelectricpointdb.org/89/UP000000589_10090_all_isoelectric_point_proteome_Mus_musculus_Mouse.html.
[39] I. Safina, M. C. Embree, *Acta Biomater.* **2022**, *143*, 26.
[40] V. V. Inamdar, S. Hao, S. B. Stephan, M. T. Stephan, *J. Controlled Release* **2024**, *370*, 310.
[41] D. K. Y. Zhang, J. M. Brockman, K. Adu-Berchie, Y. Liu, Y. Binenbaum, I. de Lázaro, M. C. Sobral, R. Tresa, D. J. Mooney, *Nat. Biomed. Eng.* **2024**, *9*, 268.
[42] A. Sechi, A. Dardis, B. Bembi, *Ther Clin Risk Manag* **2016**, *12*, 53.
[43] O. Boyman, J. Sprent, *Nat. Rev. Immunol.* **2012**, *12*, 180.
[44] W. Liao, J. X. Lin, W. J. Leonard, *Immunity* **2013**, *38*, 13.
[45] B. J. Kwee, B.o R.i Seo, A. J. Najibi, A. W. Li, T.-Y.u Shih, D. White, D. J. Mooney, *Sci. Adv.* **2019**, *5*, aav6313.
[46] J. Lou, C. Meyer, E. B. Vitner, K. Adu-Berchie, M. T. Dacus, G. Bovone, A. Chen, T. To, D. A. Weitz, D. J. Mooney, *Adv. Mater.* **2024**, *36*, 2309860.